# Surface slope tolerances: the transition from geometric raytracing to scalar wave theory

John R. Rogers
Synopsys Inc., 199 S. Los Robles Ave., Pasadena, CA 91107

## ABSTRACT

In a previous presentation, the author presented a method of tolerancing mid-frequency surface ripple, based on a sensitivity parameter that related the slope error on the surface to the ray deviation at the image plane. The method established an upper allowable limit for the slope error on the surface. Because the analysis method was based on geometric raytracing, it included no consideration of scale. (Snell's law is Snell's law, regardless of the size of the feature.) Although the intention was to apply this design method only to macroscopic surface features, the notion of a slope limit without a scale limitation raises the question as to the region of validity, i.e., when do we need to take diffraction or scatter into account? In this presentation, we examine the transition between geometric raytracing and scalar diffraction theory. This is entirely analogous to the transition between the geometric model of a Ronchi test and that of a diffraction-based, lateral shear interferometer.

**Keywords:** slope error, mid spatial frequency, error budget

## 1. INTRODUCTION

Using the laws of geometrical optics, the relationship between the displacement of a ray at the image plane, and the slope error at any surface, may be shown to be[1,2]

$$\delta y_i = \mathcal{S}_s \beta_s \tag{1}$$

where $\beta_s$ is the slope perturbation of the surface in question, and the sensitivity $\mathcal{S}_s$ of the surface is given by:

$$\mathcal{S}_s = \frac{-y_s \Delta n_s}{n'_i u'_i}. \tag{2}$$

where further $y_s$ and $\Delta n_s$ represent the beam semi-diameter and index change at the surface, and the denominator is the numerical aperture at the image plane.

Assuming the designer can decide upon a maximum allowable ray departure (either in the peak-to-valley or PV sense or in the root-mean-square, or RMS sense) then this sensitivity parameter can be used to develop an error budget for slope errors on the surface. The error budget is based on the assumption that the errors of the individual surfaces combine in the root-sum-square or RSS manner. We will refer to a surface to which a tolerance has been set as a "slope-limited" surface.

Although the approach described above is useful, it suffers from two conceptual difficulties that both arise from the fact that the entire approach is based on the use of geometric optics. First is the region of applicability: to what range of spatial frequencies can or should the approach be applied? This question was the subject of a recent paper[2] in which the fall-off of diffraction efficiency with frequency was studied for the specific case of slope-limited surfaces. Inherent in this approach is the assumption that the surface error can be decomposed into constituent sinusoidal frequencies.

The second problem is even more worrisome: the geometric approach predicts that for any sinusoidal surface error, the maximum ray deflection at the surface (and therefore the maximum ray displacement at the image plane) is determined entirely by the slope of the sinusoid at its steepest point. In principle, the same upper limit may be applied to the peak slope of a sinusoid of all frequencies; this is equivalent to requiring that the amplitude of the sinusoid diminish inversely

Tribute to James C. Wyant: The Extraordinaire in Optical Metrology and Optics Education,
edited by Virendra N. Mahajan, Daewook Kim, Proc. of SPIE Vol. 11813, 118130Q
 · doi: 10.1117/12.2567548

with the frequency. Geometrical optics predicts that in such a case, the ray deflection at the surface is bounded, because the peak slope is bounded. On the other hand, if we consider the surface to be a phase diffraction grating, then the propagation angle of the diffracted light is predicted to increase monotonically with increasing spatial frequency. Moreover, for a fixed frequency there will be some order number for which the diffraction angle exceeds the prediction of Snell's Law. This apparent disagreement is the subject of this paper.

## 2. GEOMETRICAL OPTICS VERSUS PHYSICAL OPTICS

Geometrical optics not only predicts that no rays will be refracted beyond a certain angle; it also predicts that more rays will be refracted near the maximum angle, as is shown in Figure 1.

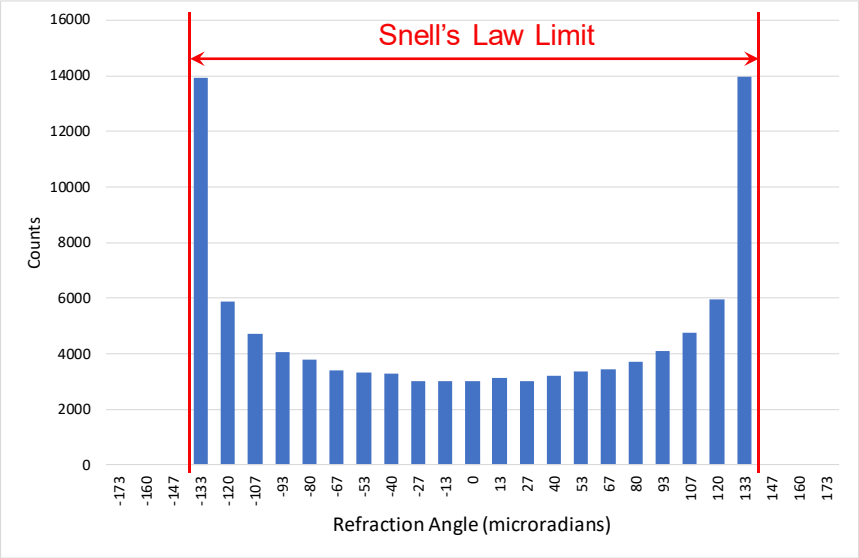


Figure 1. Histogram of ray locations for a surface having a sinusoidal surface error

The histogram shown in Figure 1 results from tracing rays at 100,000 randomly selected locations on a reflective surface having a sinusoidal surface error that was 0.557 microns in amplitude and a period of 50 mm. The resulting surface slope is bounded between +70 microradians and -70 microradians. Since the surface is reflecting, the reflected rays are bounded between +140 microradians and -140 microradians. The high values at the extremes can be understood by imagining a ray sweeping across the sinusoidal surface: the output angle varies periodically, with more dwell time near the extrema than near the center of the pattern.

## 3. DIFFRACTION ANGLE

Scalar Wave Theory predicts that any diffracted light will be sent into angles that increase monotonically with increasing spatial frequency. At some frequency or for some order number, the diffraction angle will exceed the ray deflection angle predicted by Snell's Law. This appears to be a fundamental (and potentially significant) disagreement between the geometric and physical optics calculations. In this section we examine this apparent disagreement.

For our purposes here, it suffices to consider the wavefront transmitted through a surface having a sinusoidal surface error. (The undulation of the wavefront is simply related to the undulation of the surface by the index change at the surface.) This wavefront is of the form:

$$\Phi(\mathrm{x}) = e^{i\mathrm{W}(\mathrm{x})} \tag{3}$$

where

$$\mathrm{W}(\mathrm{x}) = \mathrm{A}\sin(2\pi\xi x). \tag{4}$$

The slope (tangent of the normal) of the wavefront is

$$\mathrm{W}'(\mathrm{x}) = 2\pi\xi\mathrm{A}\cos(2\pi\xi x) \tag{5}$$

and the peak slope, i.e., the direction of the maximum ray direction angle predicted by Snell's Law, is:

$$W'(x)_{max} = 2\pi\xi A. \tag{6}$$

Next, we consider the same sinusoidal wavefront from the point of view of diffraction from a phase grating. For light that is incident normally to the substrate, the diffraction angles of the various orders are given by:

$$\sin\theta_m = m\lambda\xi \tag{7}$$

At this point it is useful to calculate the (possibly non-integer) order number that diffracts light in the same direction as the maximum predicted by Snell's Law. We will refer to this as the "Geometric Equivalent Order" (GEO) for the sinusoid. Since tolerance-level slope errors are small (typically microradians) we may equate the tangent of Equation 6 with the sine of Equation 7, yielding

$$GEO = 2\pi A/\lambda. \tag{8}$$

In most cases, GEO works out to be a non-integer value, meaning that an integer number of orders fall inside the prediction of Snell's Law, and the remaining orders are outside that predicted limit.

As mentioned above, there is an apparent disagreement between the bounded prediction of Snell's Law and the unbounded set of diffraction angles predicted by Scalar Wave Theory. The only possibility for the two theories to even approximately agree is if the diffraction efficiencies for all orders above GEO are zero or nearly zero.

For any sinusoidal grating, the diffraction efficiency into order *m* is given by[3,4]

$$\eta_m = {J_m}^2(\Delta\phi) \tag{9}$$

Where $\Delta\phi$ is the phase amplitude (half the peak-to-valley value), expressed in radians. The quantity *A* of Equation 4 is the amplitude of the transmitted sinusoidal wavefront, in length units. Dividing by the wavelength and multiplying by $2\pi$ gives the phase amplitude in radians:

$$\Delta\phi = 2\pi A/\lambda. \tag{10}$$

Comparing to Equation 8 we see the somewhat surprising fact that

$$\Delta\phi = GEO, \tag{11}$$

i.e, the argument of the Bessel functions in Equation 9 is numerically equal to the Geometric Equivalent Order for the sinusoid. Thus, we have:

$$\eta_m = {J_m}^2(\mathrm{GEO}). \tag{12}$$

## 4. EXAMPLE 1

Consider a reflective surface that suffers a sinusoidal ripple with a period of 50 mm and a peak slope of 70 microradians. We will use 550 nm for the wavelength in this example. The surface deformation is of the form:

$$Z(x) = A_{surface}\sin(2\pi\xi x). \tag{13}$$

The slope is given by

$$Z'_x = 2\pi\xi A_{surface}\cos(2\pi\xi x) \tag{14}$$

having a peak value of $2\pi\xi A_{surface}$. This peak value is 70 microradians, and we can solve to obtain the amplitude of the surface height, which is 0.557 microns (approximately one wavelength). Because this is a reflective surface, the index change at the surface is 2, and the wavefront is given by:

$$W(x) = 2A_{surface}\sin(2\pi\xi x) \tag{15}$$

or

$$W(x) = A_{wavefront} \sin(2\pi\xi x) \quad (16)$$

where $A_{wavefront}$ = 1.114 microns, or 2.025 wavelengths. The phase amplitude is therefore 2.025 waves, or 12.72 radians. From Equation 11 the Geometric Equivalent Order is also equal to 12.72, so we expect to see 12 diffraction orders inside the maximum angle predicted by Snells Law, with the remaining orders falling outside the Snell's Law prediction. The prediction of Snell's Law can be found by multiplying the peak surface slope of 70 microradians by the index difference of 2.0 to obtain 140 microradians. Figure 2 shows the diffraction efficiencies for the first ±28 orders for this sinusoid.

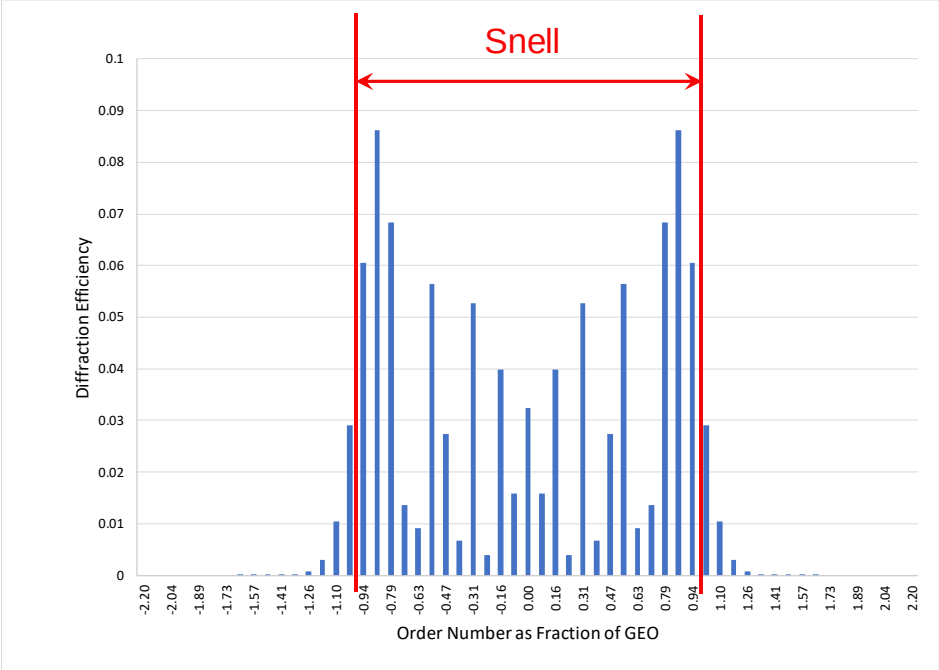


Figure 2. Diffraction efficiencies for various orders

As expected, the first 12 orders fall within the predicted limit of Snell's Law. It can be seen that the strongest diffraction occurs for orders just inside the Snell's Law prediction, and that very little diffraction occurs outside the Snell's Law prediction.

Figure 3 shows the diffraction efficiencies for a wider range of orders, on a logarithmic scale. The diffraction efficiencies fall off rapidly, beginning at the prediction of Snell's law.

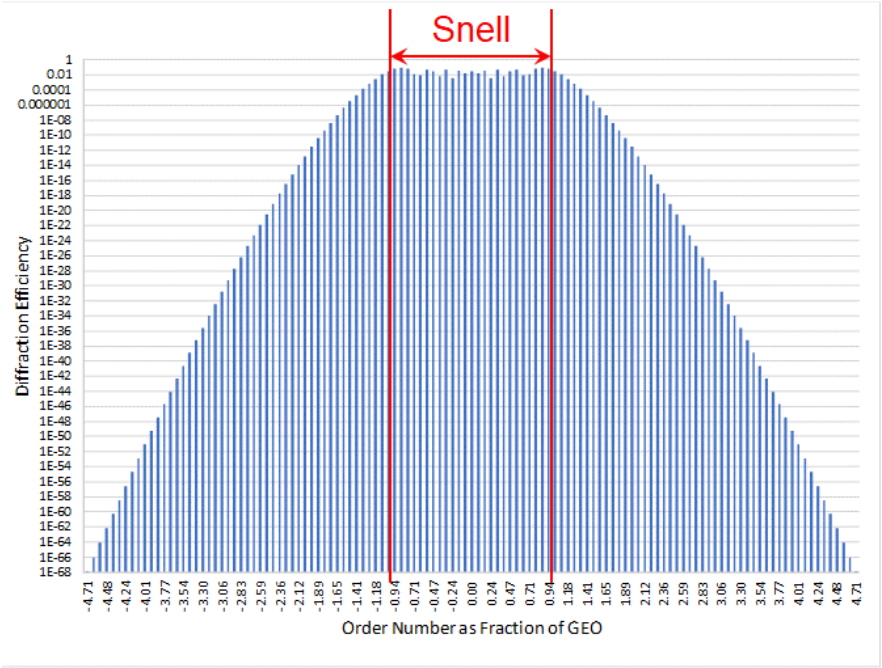


Figure 3 Diffraction efficiencies on a logarithmic scale.

Figure 4 shows a CODE V™ simulation of the diffraction from the surface in question. For reference, the optical model comprised a reflective surface with a sinusoidal deformation applied in the horizontal direction, plus a weak cylindrical lens oriented so that the diffracted light would be spread slightly in the vertical direction.

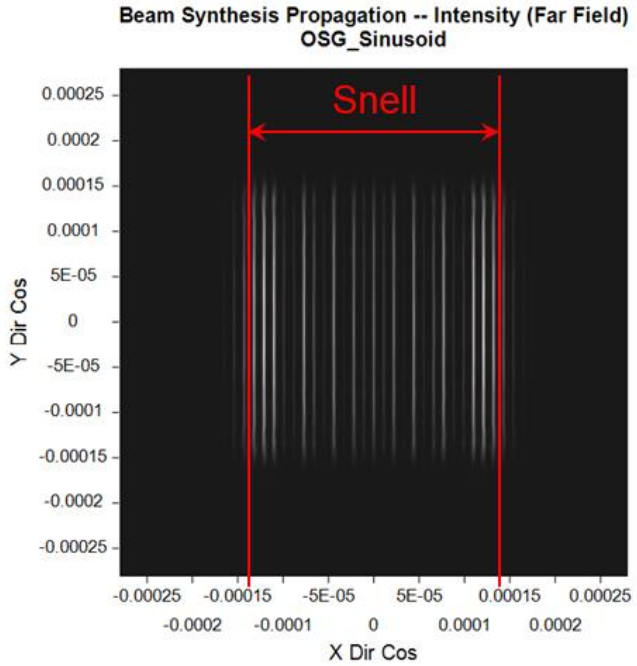


Figure 4. Simulated far field diffraction pattern for Example 1.

The simulation was carried out using the CODE V® Beam Synthesis Propagation (BSP) feature, with the results plotted in the far field. This is a beamlet-based simulation method, not based on Fourier theory and without any "knowledge" of

the concept of orders. The figure shows excellent agreement with Figure 2, with almost no energy outside the prediction of Snell's Law.

The fact that the diffraction efficiency decreases rapidly outside the prediction of Snell's Law is not coincidental but derives directly from Equation 11 and the behavior of the Bessel functions, the first 20 of which are shown in Figure 5.

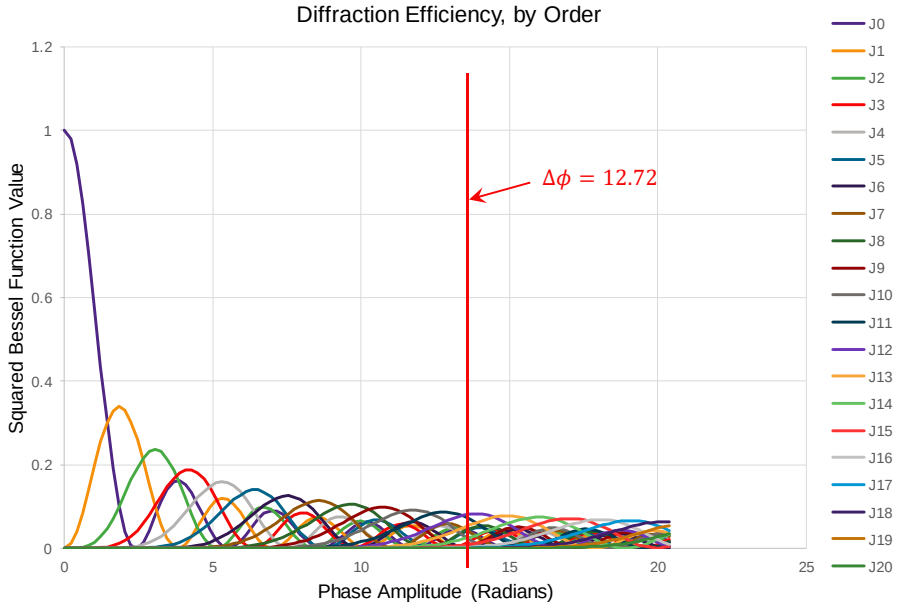


Figure 5. Squares of the first 20 Bessel Functions

It can be seen that the peak values of the Bessel function decrease with order number; however, this alone does not explain the rapid fall-off outside the prediction of Snell's Law. For this diffraction problem, the phase amplitude of the grating is 12.72 radians, indicated by the red line in the figure. According to Equation 11, the first 12 orders lie inside the prediction of Snell's Law, and we are interested in Orders 13 and higher. We therefore drop Orders 0 – 12 and re-plot the higher orders in Figure 6 at an expanded scale.


Figure 6. The Diffraction Orders outside the Snell's Law prediction.

The diffraction efficiencies for the various orders are given at the points where the Bessel Functions cross the $\Delta\phi = 12.72$ line. Order 13 (just barely outside the prediction of Snell's Law) has an efficiency of about 6%, and the diffraction efficiencies for the higher orders fall very rapidly from that value. This happens not because the *peaks* of the Bessel functions decrease with order number, but because *onsets* of the Bessel functions move to the right as the order number increases, and therefore the intersection with the vertical line representing the phase amplitude value rapidly becomes very small. Indeed, even at the expanded scale of this plot, the diffraction efficiencies for Orders 18 and higher are indistinguishable from zero.

To guard against the possibility that the numerical values for this example are somehow special or coincidentally "tuned" to yield a particularly good match between Snell's Law and diffraction, we consider an example with a smaller GEO value in the next section.

## 5. EXAMPLE 2

In this example, we replace the reflective surface of Example 1 with a refractive surface made of NBK7; this change reduces the phase amplitude by a factor of 3.87. All other parameters - the period, the peak surface slope and the wavelength – remain the same as in Example 1.

The geometry of the surface has not changed, so the amplitude of the surface height is 0.557 microns as before. Also, the period of the surface error remained the same, so the diffraction angles of the orders remain the same as before. However, because the index change at the surface is now 3.87x lower, the prediction of Snell's Law is reduced by that factor, from 140 microradians to 36.18 microradians. Also, while the surface remained the same, the transmitted wavefront now has an amplitude of 0.288 microns or 0.523 wavelengths. Multiplying by $2\pi$ gives us the phase amplitude, 3.29 radians.

From Equation 11 the Geometric Equivalent Order is also equal to 3.29, so we expect to see ±3 diffraction orders inside the maximum angle predicted by Snell's Law, with the remaining orders falling outside the Snell's Law prediction.

Figure 7 shows the diffraction efficiencies for the first ±7 orders for this sinusoid, and Figure 8 shows a numerical simulation of the far field diffraction pattern.

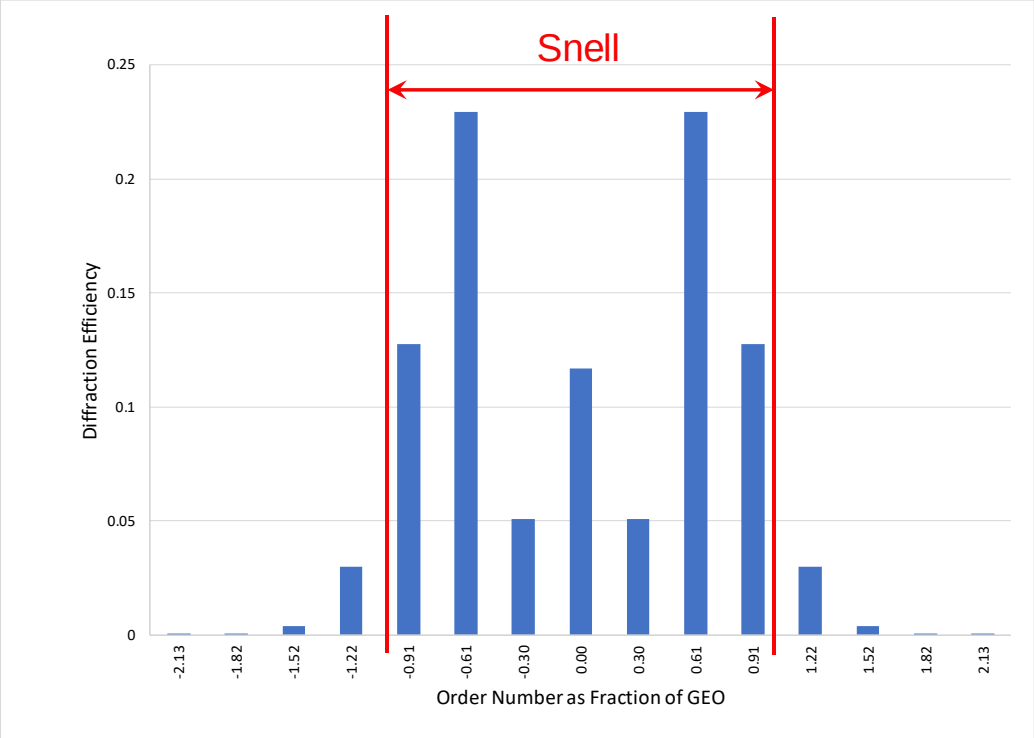


Figure 7. Diffraction Efficiencies for Example 2.

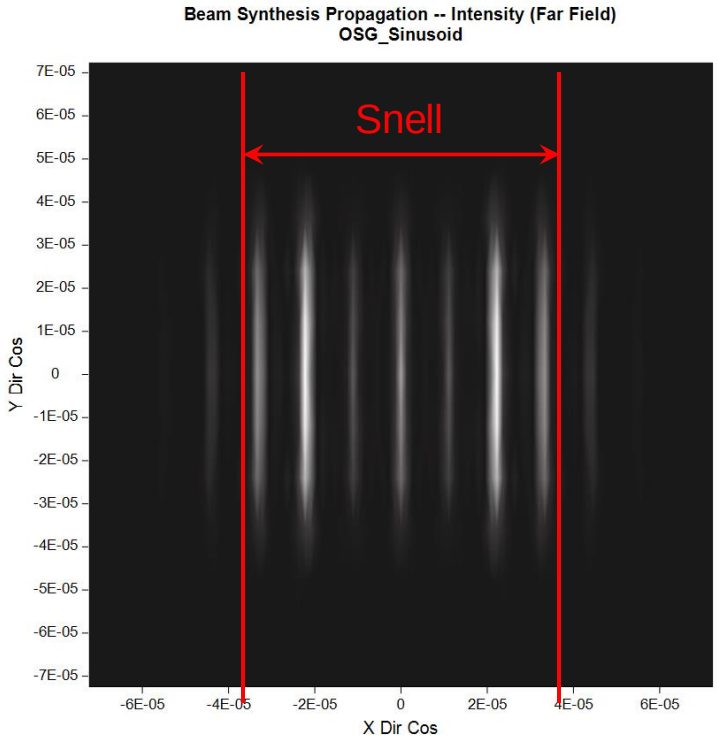


Figure 8. Simulated far field diffraction pattern for Example 2.

As before, both the calculated diffraction efficiencies and the simulated far field diffraction pattern show that almost all the energy is contained within the bounds predicted by Snell's law, with the brightest orders being near the boundary. There are ±3 orders inside the boundary, and the orders outside the boundary fall off very rapidly in diffraction efficiency.

## 6. EXAMPLE 3

In this example, we consider a case in which the GEO value is less than 1, i.e., Scalar Wave Theory predicts that all non-zero diffraction orders have diffraction angle exceeding the limit predicted by Snell's Law. It is worth noting that GEO has a value of unity when the phase amplitude has a value of one radian, or $1/2\pi$ wavelengths. The PV value is therefore $1/\pi$ waves in that case, close to Rayleigh's "quarter-wave" criterion.

The parameters of this case are the same as in Example 2, except we reduce the period by a factor of 4, from 50 mm to 12.5 mm. The frequency is therefore 0.08 cy/mm. The peak surface slope for this problem remains 70 microradians as in Example 2, and because the index change is the same, the prediction of Snell's Law remains the same, i.e., 36.18 microradians.

Because the peak surface slope remained the same while the frequency was increased by a factor of 4, the amplitude of the surface sinusoid is reduced by that factor, from 0.557 microns to 0.139 microns. Multiplying by the index change (0.5168) gives the amplitude of the wavefront, 0.072 microns, or 0.131 waves. Multiplying by $2\pi$ gives the phase amplitude, 0.822 radians. From Equation 11, the Geometric Equivalent Order is also 0.822.

From the above, we know that only the zeroth order falls within the ±36.18 microradian prediction of Snell's Law. Indeed, Scalar Wave Theory predicts the first order diffraction angle to be 44 microradians. Figures 9 and 10 show the calculated diffraction efficiencies and simulated far field patterns for this case.

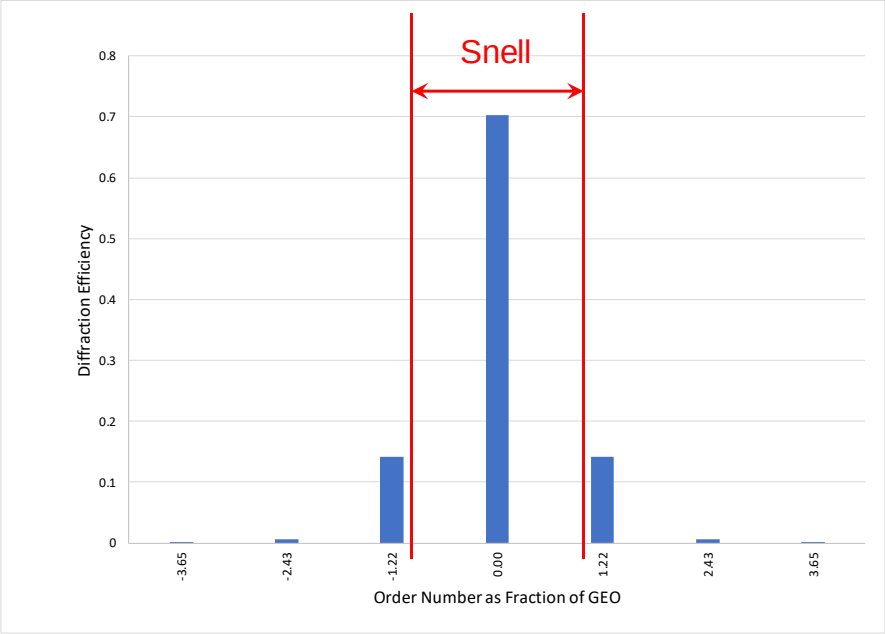


Figure 9. Diffraction Efficiencies for Example 3.

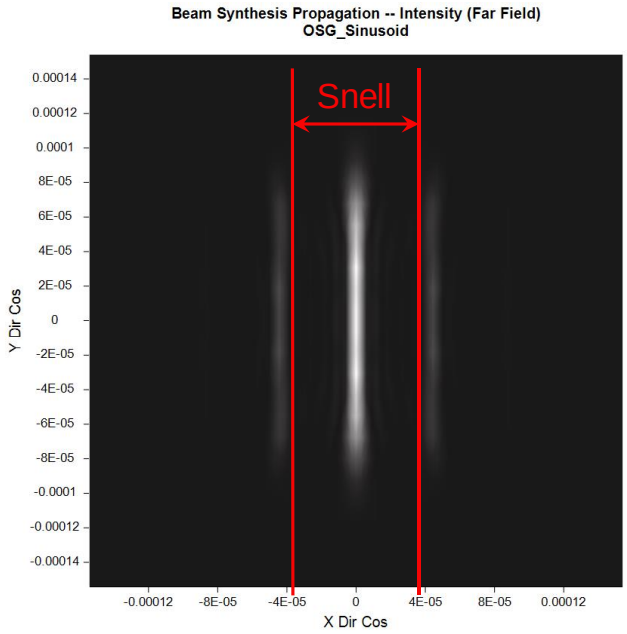


Figure 10. Simulated far field diffraction pattern for Example 3.

In this case, we see that although all the non-zero diffraction orders lie outside the prediction of Snell's Law, the diffraction efficiencies are quite weak except for Order 1 which lies just outside the Snell's Law limit.

One might imagine that once the surface slope becomes small enough that the prediction of Snell's Law is less than the first order diffraction angle (i.e., that GEO<1), no further change to the diffraction pattern would take place as the surface slope is further reduced. The following example shows that this is not the case.

## 7. EXAMPLE 4

In this example, we alter the geometry of Example 3 by reducing the surface slope by a factor of 2, from 70 microradians to 35 microradians. The prediction of Snell's Law thereby reduces by a factor of 2, from 36.18 to 18.09. The glass remains NBK7, the wavelength remains 550 nm, and the surface period remains 12.5 mm.

Because the period of the sinusoid has not changed, the first order diffraction angle remains 44 microradians. However, in this case the surface amplitude is reduced by a factor of 2, from 0.139 microns to 0.0696 microns.

The amplitude of the transmitted wavefront is therefore 0.0360 microns or 0.065 waves, corresponding to a phase amplitude of 0.411 radians. From this, we know that the Geometric Equivalent Order is 0.411. Figures 11 and 12 show the diffraction efficiencies and simulated far field patterns at the same scale as Figures 9 and 10.

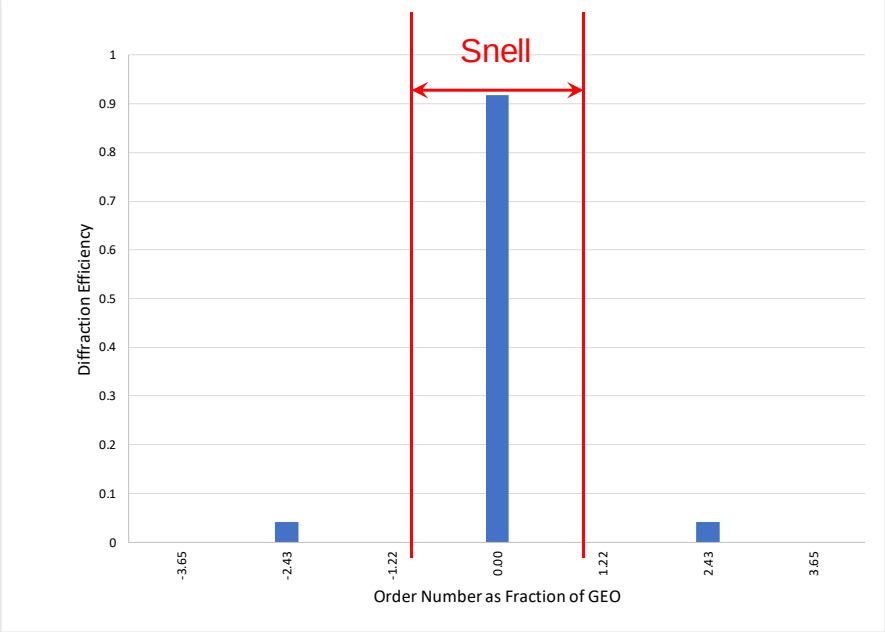


Figure 11. Diffraction Efficiencies for Example 4.

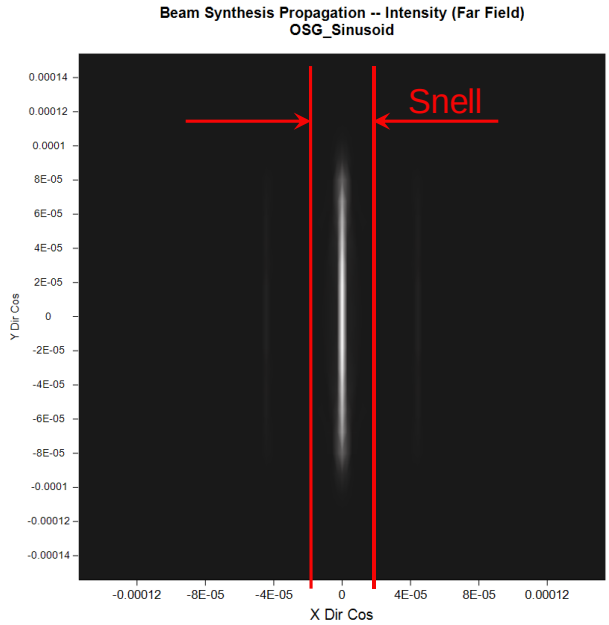


Figure 12. Simulated far field diffraction pattern for Example 4.

In this case, we decreased the slope of the surface without changing the period of the surface error. Because the surface period remained the same, the positions of the diffracted orders remained the same; what changed was the efficiencies of the diffracted orders, because they now lie farther from the region predicted by Snell's Law. Just as in the last example, the number of orders within the Snell's Law prediction is one (the zeroth order), but the amount of light outside the Snell's Law prediction has decreased substantially.

## 8. EFFECTIVENESS AS A TOLERANCING TOOL

Examples 1 and 2 clearly show that Snell's Law gives a reasonable first approximation to the distribution of stray, or scattered light from surface slope errors, at least when the slope errors are relatively large. Examples 3 and 4 show that when the surface slopes are small enough that the prediction of Snell's Law is less than the first order diffraction angle, there is still some benefit to tightening the surface slope tolerance: even though the diffraction angles don't change, the amount of diffracted energy is decreased.

It is a reasonable question to ask whether surface slope remains a useful tool for very tight tolerances. Is there a useful correlation between slope tolerance and image quality when GEO < 1? Does anything change substantially between that region and the GEO > 1 region?

To answer these questions, we examined the Strehl Ratio of 50 optical systems with different tolerances on peak slope. The optical system comprised an F/4 singlet made of NBK7. We aspherized the first surface to completely eliminate spherical aberration. We then applied randomized sinusoidal errors to the first surface, as described below. The focal length of the singlet was 200 mm, and the entrance pupil diameter was 50 mm. The Airy radius for this system is 2.68 micrometers, and the sensitivity parameter $\mathcal{S}_s$ has a value of 0.103 micrometers per microradian, from Equation 2.

To each of the optical systems in the test series, we assigned a slope tolerance $\beta_{max}$ ranging from 50 microradians to 1 microradian. For each such test system, we perturbed the optical surface simultaneously with 300 different frequencies ranging from one cycle per millimeter to one cycle per part diameter, i.e., 50 cycles per millimeter. Each such frequency component was assigned a random orientation, and the amplitude of the frequency component was chosen so that the peak slope of that component was equal to the slope tolerance $\beta_{max}$. The phase (lateral position) of each frequency component was randomized so that the surface errors did not align at the center of the part.

In the analysis, we calculated the Strehl Ratio from the RMS wavefront variance for the on-axis field point, after subtracting best-fit tilt from the transmitted wavefront. Figure 13 plots the Strehl Ratio as a function of the anticipated blur radius given by the product $\mathcal{S}_s\beta_{max}$. For the plot, we normalized the anticipated blur size to the Airy disk radius.

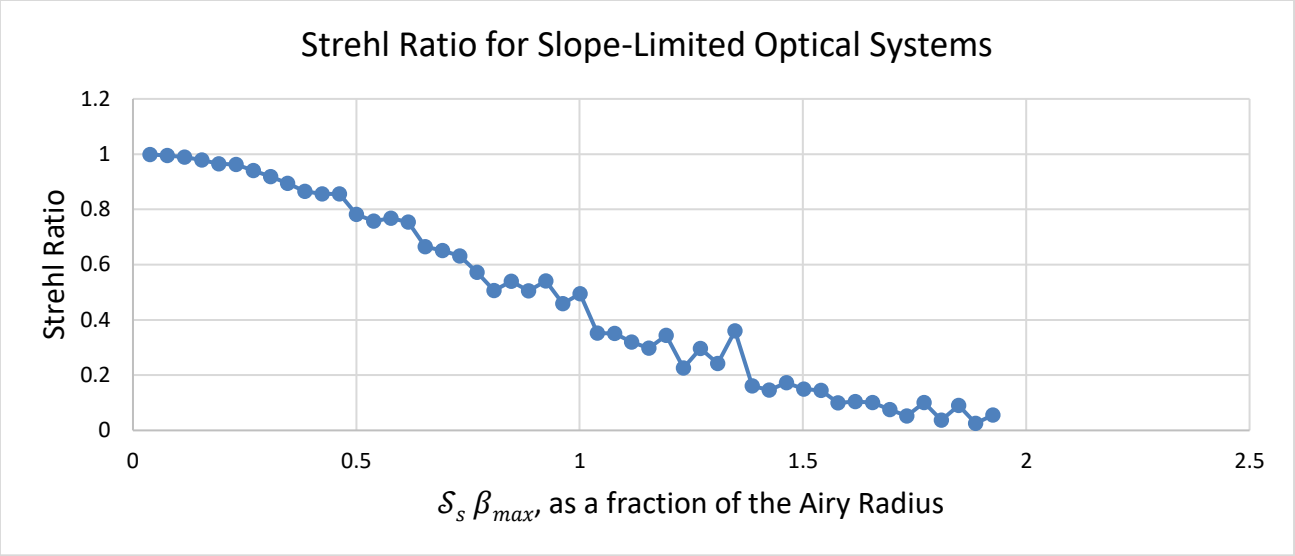


Figure 13. Strehl Ratio for a slope-limited optical system.

The figure shows some fluctuations in the Strehl ratio because of the random nature of the surface perturbation. Aside from the random fluctuations, the curve demonstrates good correlation between the $\mathcal{S}_s\beta_{max}$ product and Strehl Ratio.

## 9. CONCLUSIONS

We have shown that for sinusoidal surface errors, almost all the diffracted light remains within the bounds predicted by Snell's Law. Although it is certainly true that a detailed simulation of the diffracted light requires Scalar Wave Theory, a reasonable first estimate of the scattered light distribution can be obtained simply by applying Snell's Law and assuming that the light is refracted by the sinusoidal surface. The number of diffraction orders within the boundaries predicted by Snell's Law is equal to the phase amplitude (in radians) of the transmitted wavefront. Good correlation exists between the slope tolerance and Strehl Ratio.

## REFERENCES

1. Rogers, J. R., "Slope Sensitivities for Optical Surfaces" Proc. SPIE. 9582, Optical System Alignment, Tolerancing, and Verification IX, 958206 (2015).
2. Rogers, J. R., "Surface Slope Error Tolerances: Applicable Range of Spatial Frequencies" International Optical Design Conference paper IW4A1, (2021).
3. C. V. Raman and N. S. Nagendra Nath, "The diffraction of light by high frequency sound waves: Part I." Proc. Indian Acad. Sci., Sect. A **2**, 406–412 (1935).
4. Burckhardt, C. B., Collier, R. J., and Lin, L.H., [Optical Holography], Academic Press, New York, (1971).